Supplementary Information

Breaking the speed limit in two-photon microscopy via deep-learning imaging reconstruction from anisotropic sparse sampling

Ang Xuan[1], Yuanjie Gu[1], Yiqun Wang[1], Jianping Wang[1], Chengyu Li[2], Su Tang[3], Yao Wu[4], Cihang Kong[2,*], Biqin Dong[1,*]

[1] College of Biomedical Engineering, Yiwu Research Institute, Fudan University, Shanghai, China
[2] Institute for Translational Brain Research, Fudan University, Shanghai, China
[3] Department of Anesthesiology, Fudan University Shanghai Cancer Center, Shanghai, China
[4] MicroLux (Shanghai) Intelligent Science & Technology Co., Ltd., Shanghai, China
[*]**Corresponding authors:** B.D. (dongbq@fudan.edu.cn) and C.K. (kongcihang@fudan.edu.cn)

Supplementary Figure 1. Various scanning imaging strategies and upsampling methods.

Supplementary Figure 2. Comparison of stimulated neurons image reconstruction from isotropic and IRIS downsampling via interpolation.

Supplementary Figure 3. Simulation of IRIS for fluorescence microsphere imaging compared with the experimental results.

Supplementary Figure 4. Network architecture of IRIS.

Supplementary Figure 5. The impact of filled noise on the quality of image reconstruction.

Supplementary Figure 6. Performance upsampling by synthetic shapes.

Supplementary Figure 7. Performance and segmentation on super-resolution by stimulation data.

Supplementary Figure 8. Comparison of isotropic downsampling and anisotropic downsampling using the IRIS-upsampling method.

Supplementary Figure 9. Comparison of results with different upsampling rates of IRIS methods.

Supplementary Figure 10. IRIS reconstruction of time series data.

Supplementary Figure 11. IRIS reconstruction of the neuron simulation data of voltage probe.

Supplementary Figure 12. The full trace and spike inference of Figure 4c.

Supplementary Figure 13. IRIS applied to vascular flow velocity imaging.

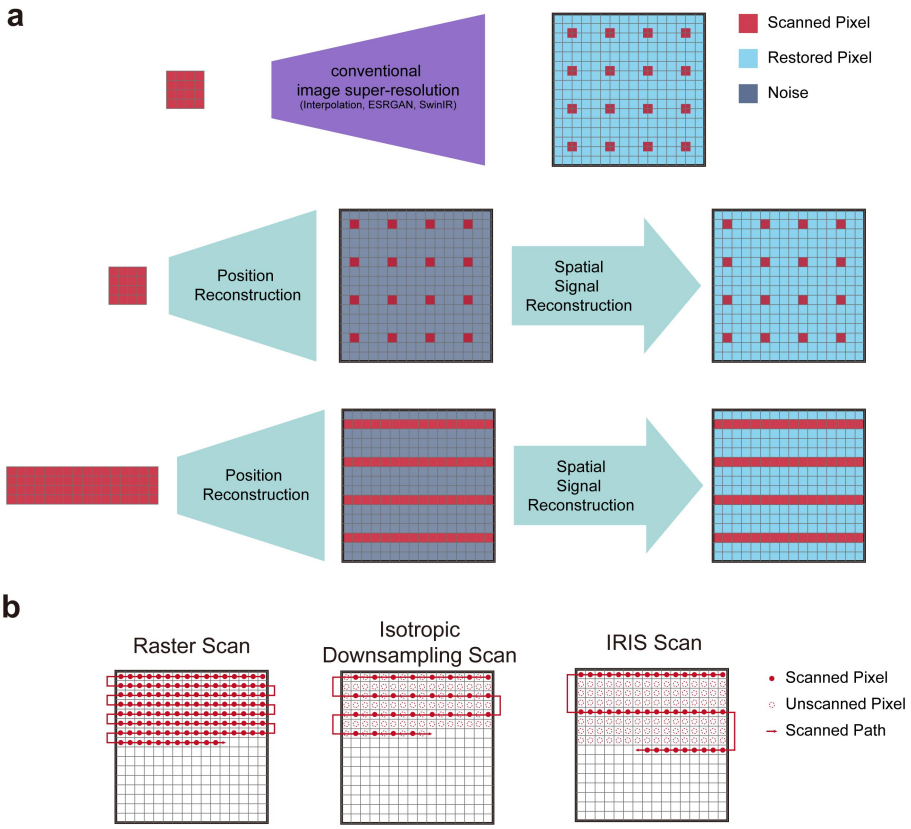

Supplementary Figure 1. Various scanning imaging strategies and upsampling methods. a. Conventional upsampling, IRIS-based isotropic upsampling, and IRIS upsampling strategies. b. Raster scan, isotropic downsampling scan, and IRIS scan imaging strategies.

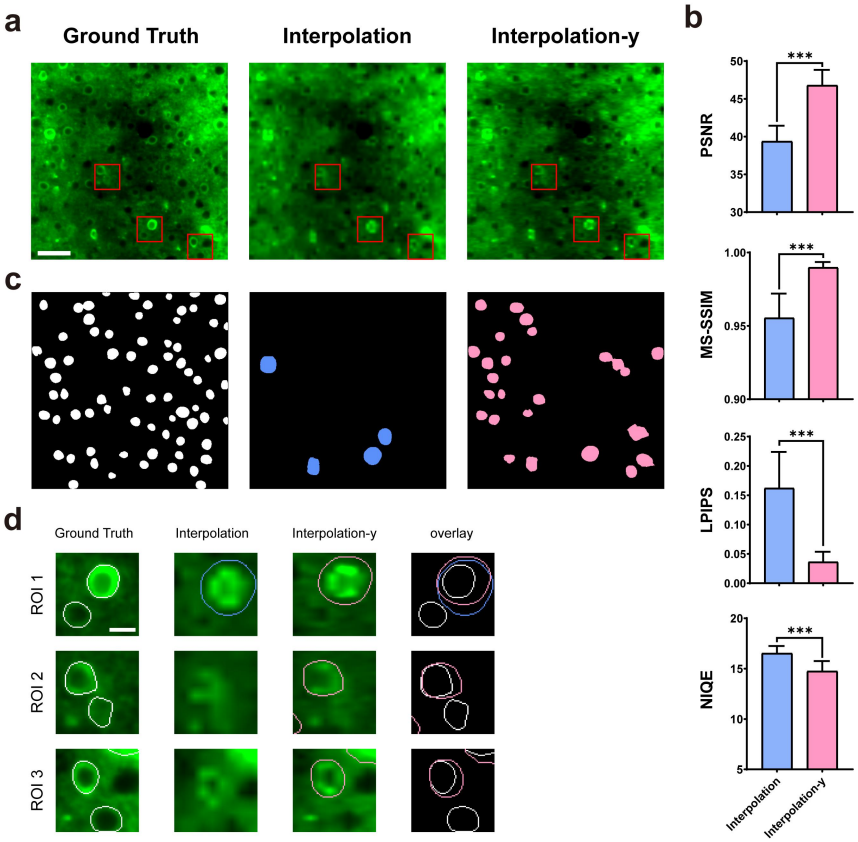

Supplementary Figure 2. Comparison of stimulated neurons image reconstruction from isotropic and IRIS downsampling via interpolation. a. Reconstructed results of isotropic downsampling and IRIS downsampling via interpolation. Scale bar, 50 μm. b. The image evaluation metrics of these two reconstruction methods. c. Neuron segmentation results by CellSAM, from left to right are the ground truth (GT), interpolation and interpolation-y. d. Example neurons, zoomed in from the boxed regions in b-g, illustrating segmentation results across different upsampling methods, overlaid with the segmented neuron boundaries. Scale bar, 5 μm.

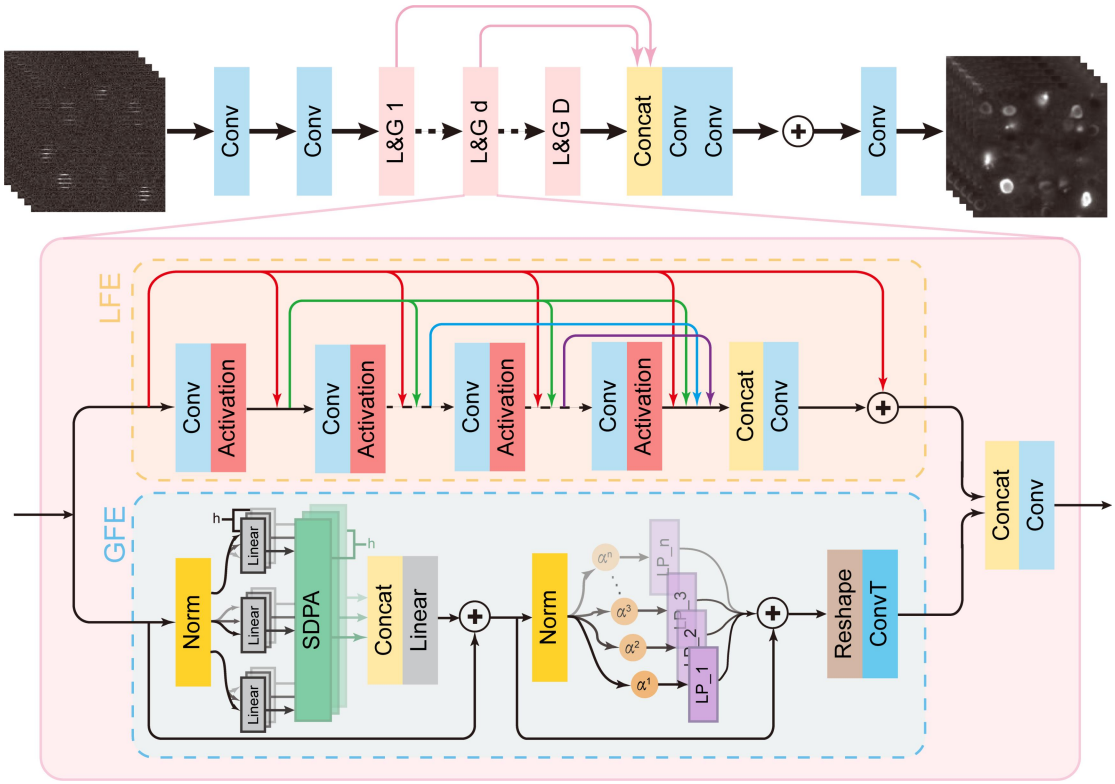

Supplementary Figure 3. Network architecture of IRIS. Conv: convolution, FE: feature extraction, Concat: concatenation, LEF: local feature extraction, GEF: global feature extraction, Norm: normalization, SDPA: scaled dot-product attention.

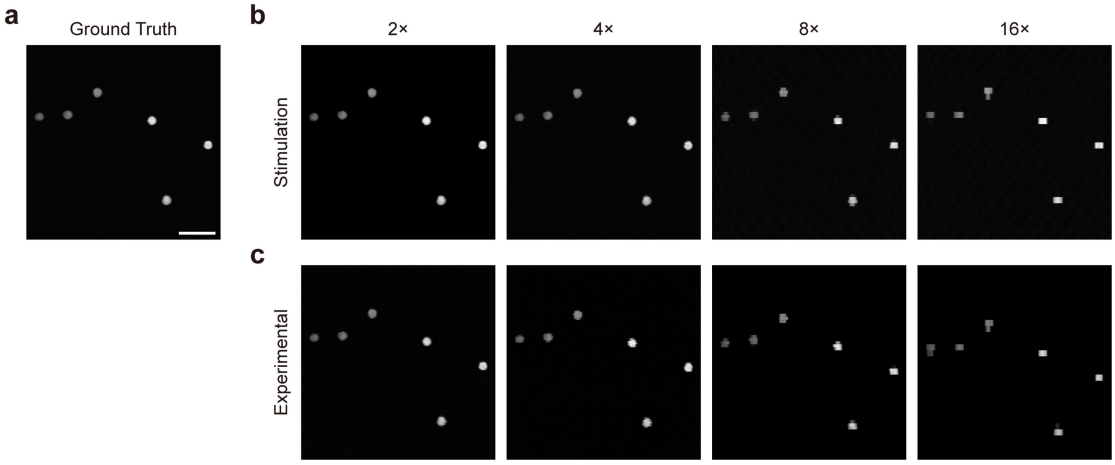

Supplementary Figure 4. Simulation of IRIS for fluorescence microsphere imaging compared with the experimental results. a. 512×512 full-pixel imaging of fluorescent microspheres. b. Downsampling based on different magnification ratios in a. c. Experimental results of downsampling ratios under different IRIS scan ratio.

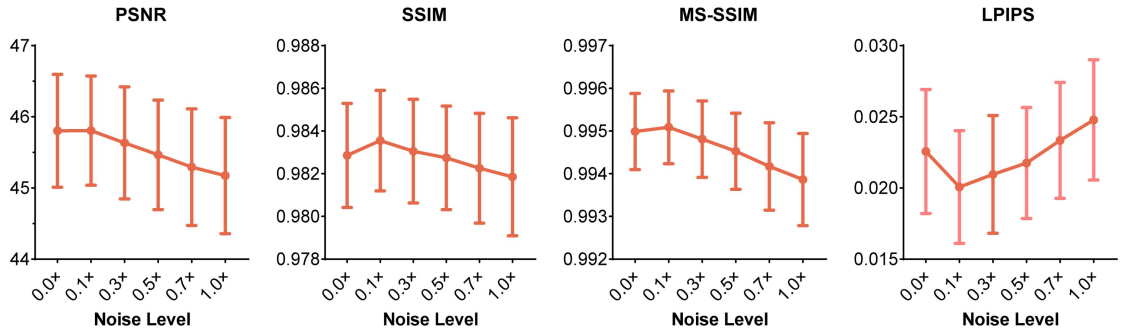

Supplementary Figure 5. The impact of filled noise on the quality of image reconstruction. Gaussian noise at levels of 0.0× (noise-free), 0.1×, 0.3×, 0.5×, 0.7×, and 1.0× was applied to evaluate the reconstruction quality of synthetic shapes data by IRIS methods.

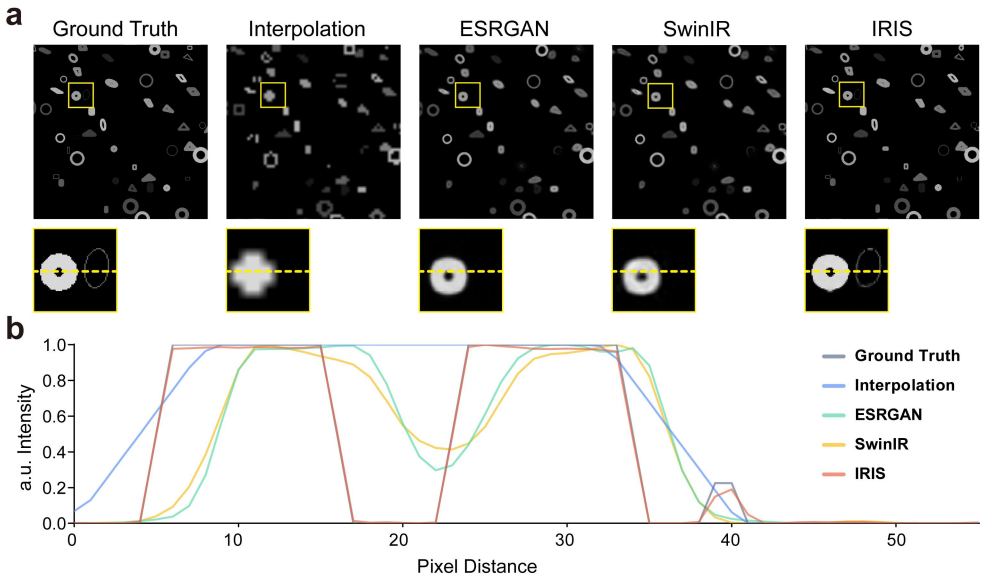

Supplementary Figure 6. Performance upsampling by synthetic shapes. a. Reconstruction on synthetic shapes. From left to right are the ground truth (GT), interpolation, ESRGAN, SwinIR and IRIS results. Magnified views of the boxed regions are the detail of image. b. The intensity distribution along the dashed line regions in a are shown. The gray curve represents the intensity distribution of the GT image, while the blue, green, yellow and red curve shows the distribution after super-resolution with interpolation, ESRGAN, SwinIR and IRIS, respectively.

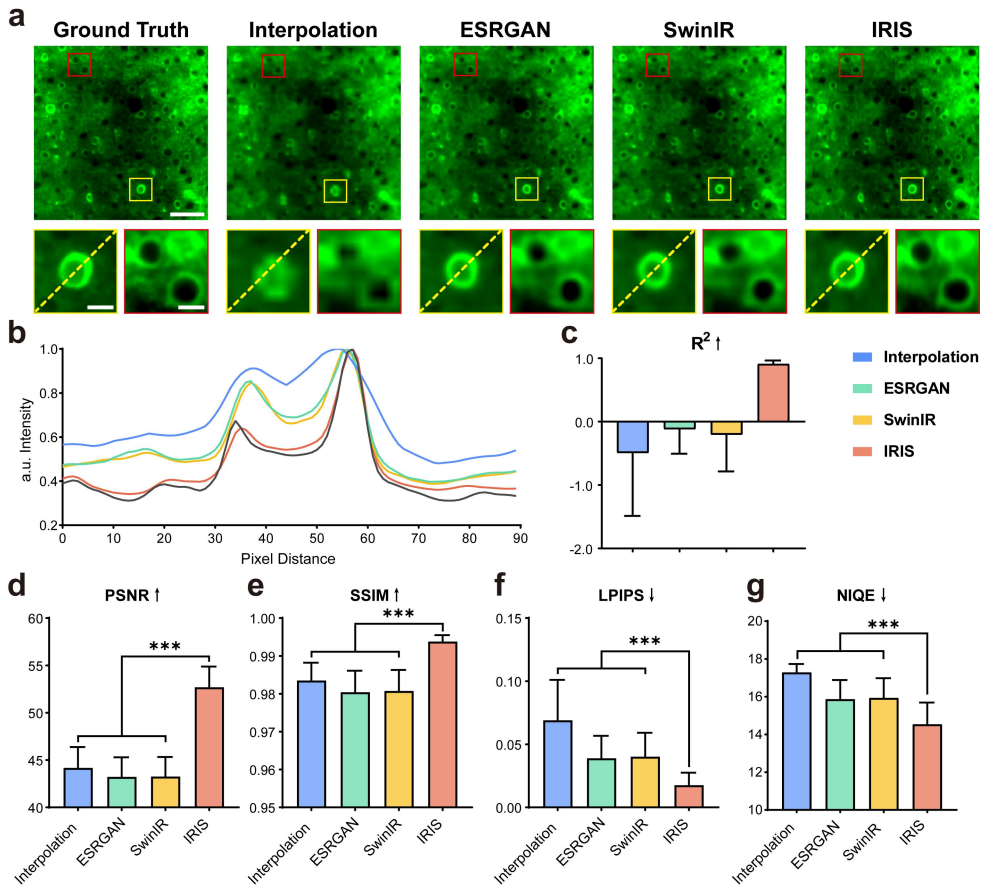

Supplementary Figure 7. Performance and segmentation on super-resolution by stimulation data. a. Reconstruction on stimulation neurons image. From left to right are the ground truth (GT), interpolation, ESRGAN, SwinIR and IRIS results (Scale bar, 50 μm). Magnified views of the boxed regions are the detail of image (Scale bar, 5 μm). b. The intensity distribution along the dashed line regions in a are shown. The gray curve represents the intensity distribution of the GT image, while the blue, green, yellow and red curve shows the distribution after super-resolution with interpolation, ESRGAN, SwinIR and IRIS, respectively. c. The fitting degree of the intensity curve obtained by the super-resolution method and the GT curve. d-g. The image evaluation metrics of super-resolution methods, including PSNR, SSIM, MS-SSIM and LPIPS.

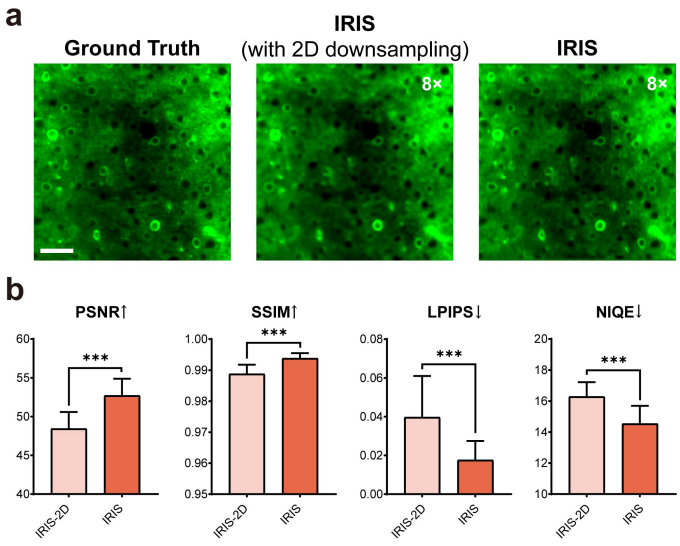

Supplementary Figure 8. Comparison of isotropic downsampling and anisotropic downsampling using the IRIS-upsampling method. a. Reconstruction on stimulation neurons image. b. The image evaluation metrics of super-resolution methods, including PSNR, SSIM, LPIPS and NIQE.

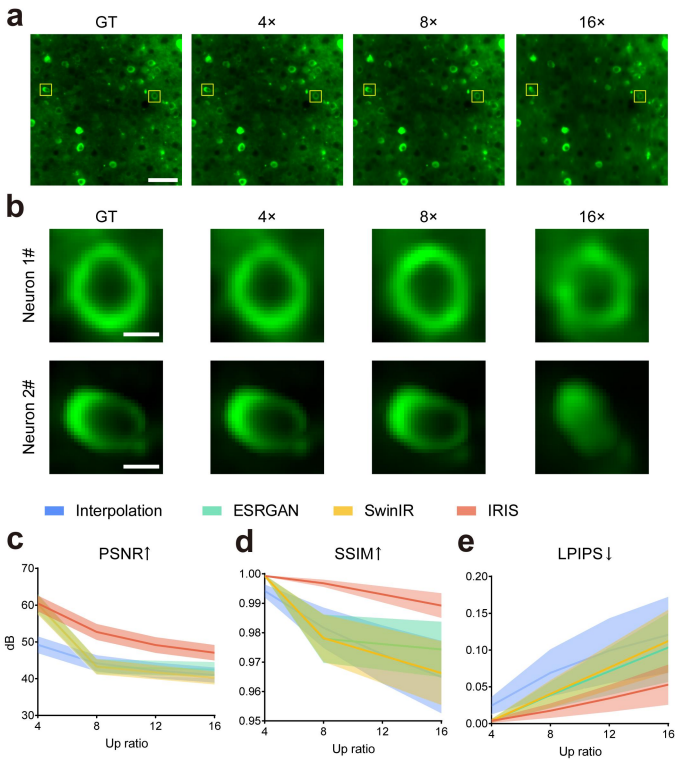

Supplementary Figure 9. Comparison of results with different upsampling rates of IRIS methods. a. Reconstruction on stimulation neurons image by different downsamlping rate. b. Magnified views of the single neuron in a. c-e. The image evaluation metrics of image reconstruction methods with different rate, including PSNR, SSIM and LPIPS.

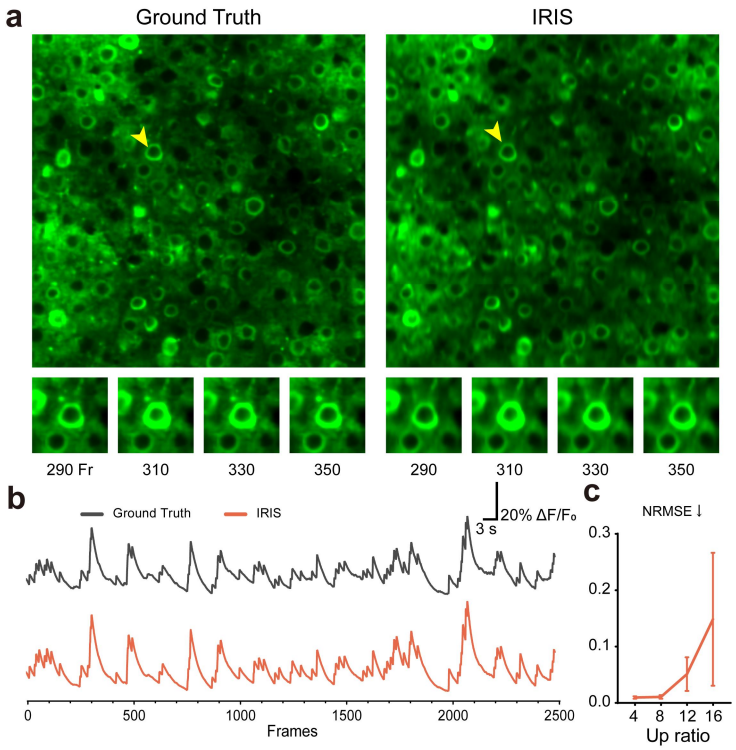

Supplementary Figure 10. IRIS reconstruction of time series data. a. Comparison of GT and IRIS reconstructions of neuronal simulation data. b. Comparison of the fluorescence curves of neuron (arrow in a) between GT and IRIS. GT: gray, IRIS: red. c. The relationship between the fluorescence curve and the upsampling factor.

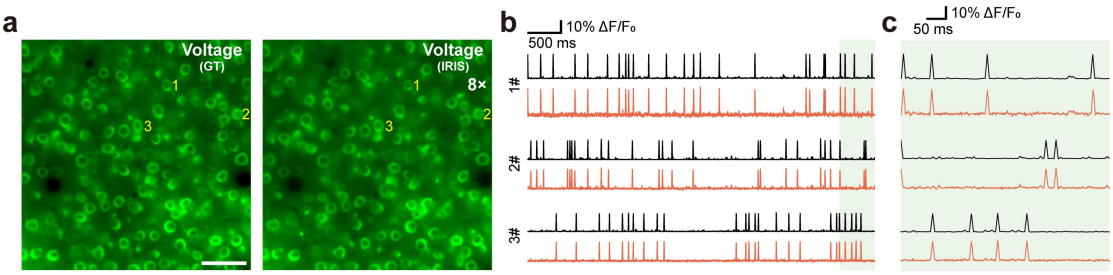

Supplementary Figure 11. IRIS reconstruction of the neuron simulation data of voltage probe. a. IRIS reconstructed and GT's MIP image. b. The activity curves of the three neurons marked in a, GT: gray, IRIS: red. c. Magnified view of the light green area in b.

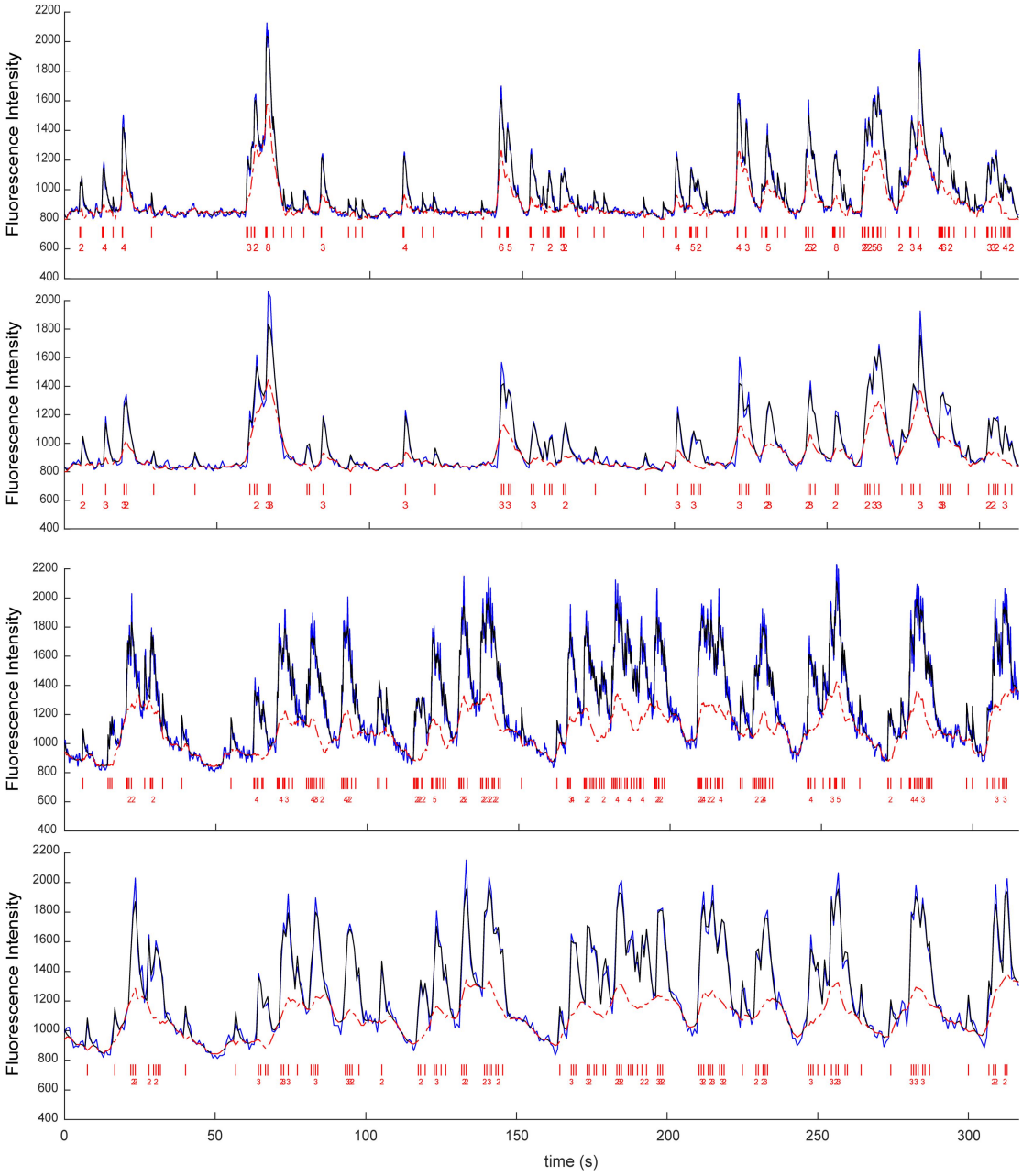

Supplementary Figure 12. The full trace and spike inference of Figure 4c. The complete time-series fluorescence intensity curve and the spike inference using MLspike (lines 1 and 3), as well as the time-downsampled fluorescence intensity curves corresponding to the full-pixel acquisition at the time resolution of the latter and the spike inference using MLspike (lines 2 and 4).

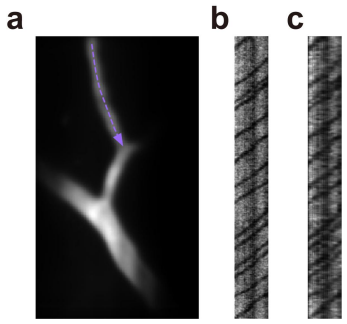

Supplementary Figure 13. IRIS applied to vascular flow velocity imaging. a. MIP of the vascular flow velocity. b-c. The velocity of the purple line in a with FAST denoised and IRIS, respectively.